Journal of Sound and Vibration (2001) **240**(2), 323–349
doi:10.1006/jsvi.2000.3233, available online at http://www.idealibrary.com on IDEAL®

NON-LINEAR DYNAMIC ANALYSIS AND CONTROL OF CHAOS FOR A TWO-DEGREES-OF-FREEDOM RIGID BODY WITH VIBRATING SUPPORT

Z.-M. Ge and P.-C. Tsen

Department of Mechanical Engineering, National Chiao Tung University, 1001 *Ta Hsueh Road, Hsinchu* 30050 *Taiwan, Republic of China*

(*Received* 21 *April* 1999, *and in final form* 12 *July* 2000)

The dynamic behaviors of a two-degrees-of-freedom rigid body with vibrating support are studied in this paper. Both analytical and computational results are employed to obtain the characteristics of the system. By using the Lyapunov direct method the conditions of stability of the relative equilibrium position can be determined. The incremental harmonic balance method (IHB) is used to find the stable and unstable periodic solutions for the strongly non-linear system. By applying various numerical results such as phase plane, Poincaré map, time history and power spectrum analysis, a variety of periodic solutions and the phenomena of the chaotic motion is presented. The effects of the changes of parameters in the system can be found in the bifurcation diagrams. Further, the chaotic behavior is verified by using Lyapunov exponents. The modified interpolated cell mapping method (MICM) is used to study the basins of attraction of periodic attractors and the fractal structure. Besides, additions of a constant torque, a periodic torque, addition of dither signals, delayed feedback control, adaptive control, and bang–bang control are used to control the chaos phenomena effectively.

1. INTRODUCTION

In the dynamics of a rigid body with a fixed point, the mechanics in question has three degrees of freedom. In engineering system, however, one often encounters a rigid body attached to the base by two-degrees-of-freedom joint, consisting of a vertical axis and a horizontal one, which are mutually perpendicular. The motion of such a system with vibration of support will be considered in the paper, where the only external moments is that of the gravitational force.

2. EQUATIONS OF MOTION

A rigid body, shown in Figure 1, has a rotating support with mutually perpendicular axes [1–3]. The motion will be described in terms of two sets of Cartestian co-ordinates: $X_1X_2X_3$ and a moving co-ordinate system $x_1x_2x_3$ rigidly attached to the rigid body, called body axis. The origin of both co-ordinate systems are at the point of intersection O of the joint axes; X_3- and x_1-axis are the fixed and moving axes of the joint, respectively. All the kinematical possibility of the body relative to the inertial co-ordinates $X_1X_2X_3$ may be described in terms of two angles: the angle α between the X_1- and x_1-axis, and the angle β between the x_2 and X_1X_2 plane. The angles α and β, which will be taken as generalized

0022-460X/01/070323 + 27 $35.00/0

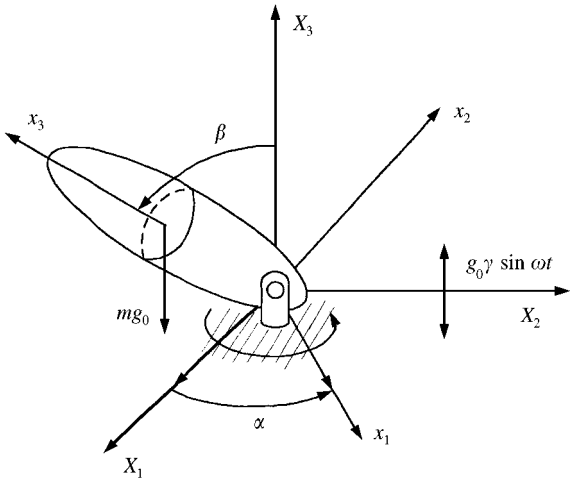

Figure 1. A schematic diagram of the rigid body.

co-ordinate, may be treated as the angles of two successive rotation through which one can transfer the rigid body from its initial position ($\alpha = \beta = 0$, the moving system of co-ordinate coincides with the fixed one) to the present position. The first rotation, through the angle α, takes place about the X_3-axis (the fixed vertical axis of the joint) and is described by the matrix

$$\Gamma_\alpha = \begin{Vmatrix} \cos\alpha & \sin\alpha & 0 \\ -\sin\alpha & \cos\alpha & 0 \\ 0 & 0 & 1 \end{Vmatrix}.$$

The second rotation, through the angle β, takes place about the x_1-axis, one of the body axes of the joint and corresponds to the matrix.

$$\Gamma_\beta = \begin{Vmatrix} 1 & 0 & 0 \\ 0 & \cos\beta & \sin\beta \\ 0 & -\sin\beta & \cos\beta \end{Vmatrix}.$$

The transformation matrix from $X_1X_2X_3$ co-ordinates to $x_1x_2x_3$ co-ordinates is the product $\Gamma = \Gamma_\alpha\Gamma_\beta$.

Let ω_i denote the projection of the angular velocity vector ω of the body onto the x_i ($i = 1, 2, 3$) axis. The kinematics equations expressing the components ω_i in the generalized co-ordinates β, and the generalized velocities $\dot{\alpha}$ and $\dot{\beta}$ are

$$\omega_1 = \dot{\beta}, \quad \omega_2 = \dot{\alpha}\sin\beta, \quad \omega_3 = \dot{\alpha}\cos\beta. \tag{1}$$

The kinetic energy of the motion of a rigid body with a fixed point is

$$T = \tfrac{1}{2}[\varpi]^{\mathrm{T}}[J][\varpi], \tag{2}$$

where $[J]$ is the inertia tensor of the body relative to the fixed point, and $[\varpi]^{\mathrm{T}} = [\omega_1, \omega_2, \omega_3]$.

Expanding the scalar product in equation (2) taking equation (1) into account, we obtain

$$KE = \tfrac{1}{2} K(\beta)\dot{\alpha}^2 + \tfrac{1}{2} J_{11}\dot{\beta} - b(\beta)\dot{\alpha}\dot{\beta}, \tag{3}$$

where

$$K(\beta) = J_{22}\sin^2\beta + J_{33}\cos^2\beta - J_{23}\sin 2\beta,$$

$$b(\beta) = J_{12}\sin\beta + J_{13}\cos\beta,$$

with J_{ii} $(i = 1, 2, 3)$ being the axial moment of inertia and $J_{ij} = J_{ji}$ $(i \neq j,\ i, j = 1, 2, 3)$ the product of inertia of the body in $x_1x_2x_3$ co-ordinates.

The potential energy of the motion of the rigid body in system $X_1X_2X_3$ is

$$PE = mg_0h(1 + \cos\beta), \tag{4}$$

where m is the mass of body, h is the distance between center of mass and the fixed point. The Lagrangian of the system has the expression

$$L = \tfrac{1}{2} K(\beta)\dot{\alpha}^2 + \tfrac{1}{2} J_{11}\dot{\beta}^2 - b(\beta)\dot{\alpha}\dot{\beta} - mg_0h(1 + \cos\beta). \tag{5}$$

The Lagrange's equation corresponding to equation (5) with damping is

$$K(\beta)\ddot{\alpha} - b(\beta)\ddot{\beta} + Z(\beta)\dot{\alpha}\dot{\beta} - J(\beta)\dot{\beta}^2 = -k_1\dot{\alpha}, \tag{6}$$

$$J_{11}\ddot{\beta} - b(\beta)\ddot{\alpha} - \tfrac{1}{2} Z(\beta)\dot{\alpha}^2 - mg_0h\sin\beta = -k_2\dot{\beta}, \tag{7}$$

where k_1, k_2 are coefficients of damping, and

$$Z(\beta) = (J_{22} - J_{33})\sin 2\beta - 2J_{23}\cos 2\beta,$$

$$J(\beta) = J_{12}\cos\beta - J_{13}\sin\beta.$$

By equations (6) and (7), we have

$$A(\beta)\ddot{\beta} + b(\beta)Z(\beta)\dot{\alpha}\dot{\beta} - b(\beta)J(\beta)\dot{\beta}^2 + b(\beta)k_1\dot{\alpha} - \tfrac{1}{2} K(\beta)Z(\beta)\dot{\alpha}^2$$
$$- K(\beta)mg_0h\sin\beta + K(\beta)k_2\dot{\beta} = 0, \tag{8}$$

$$A(\beta)\ddot{\alpha} + Z(\beta)J_{11}\dot{\alpha}\dot{\beta} - J(\beta)J_{11}\dot{\beta}^2 + J_{11}k_1\dot{\alpha} - \tfrac{1}{2} b(\beta)Z(\beta)\dot{\alpha}^2$$
$$- b(\beta)mg_0h\sin\beta + b(\beta)k_2\dot{\beta} = 0, \tag{9}$$

where

$$A(\beta) = K(\beta)J_{11} - b^2(\beta).$$

Changing the time scale to $\tau = \omega_n t$, equations (6) and (7) can be written in dimensionless form.

Define

$$\omega_n^2 = \frac{mg_0h}{J_{11}}.$$

Equations (6) and (7) become

$$\ddot{\alpha} - \frac{b(\beta)}{K(\beta)}\ddot{\beta} + \frac{Z(\beta)}{K(\beta)}\dot{\alpha}\dot{\beta} - \frac{J(\beta)}{K(\beta)}\dot{\beta}^2 + \frac{\bar{k}_1}{K(\beta)}\dot{\alpha} = 0, \tag{10}$$

$$\ddot{\beta} - \frac{b(\beta)}{J_{11}}\ddot{\alpha} - \frac{1}{2}\frac{Z(\beta)}{J_{11}}\dot{\alpha}^2 - \sin\beta + \frac{\bar{k}_2}{J_{11}}\dot{\beta} = 0, \tag{11}$$

where dot notion implies the derivative with respect to τ and

$$\bar{k}_1 = \frac{k_1}{\omega_n}, \quad \bar{k}_2 = \frac{k_2}{\omega_n}.$$

The inertial system $X_1X_2X_3$ is now subject to a vertical vibration with acceleration $\mathbf{g}_0$ $\gamma \sin \omega t$ where $\mathbf{g}_0$ is the gravitational acceleration, γ the constant and ω the given frequency of vibrating support. Then, equations (10) and (11) become

$$\ddot{\alpha} - \frac{b(\beta)}{K(\beta)}\ddot{\beta} + \frac{Z(\beta)}{K(\beta)}\dot{\alpha}\dot{\beta} - \frac{J(\beta)}{K(\beta)}\dot{\beta}^2 + \frac{\bar{k}_1}{K(\beta)}\dot{\alpha} = 0, \tag{12}$$

$$\ddot{\beta} - \frac{b(\beta)}{J_{11}}\ddot{\alpha} - \frac{1}{2}\frac{Z(\beta)}{J_{11}}\dot{\alpha}^2 - (1 + \gamma \sin \eta\tau)\sin\beta + \frac{\bar{k}_2}{J_{11}}\dot{\beta} = 0, \tag{13}$$

where $\eta = \omega/\omega_n$.

Transform the above equations into following state equations:

$$\dot{x}_1 = \frac{1}{A(x_2)}\left[\frac{1}{2}b(x_2)Z(x_2)x_1^2 + J_{11}J(x_2)x_3^2 - J_{11}\bar{k}_1x_1 - b(x_2)\bar{k}_2x_3 - J_{11}Z(x_3)x_1x_3 \right.$$

$$\left. + b(x_2)(1 + \gamma \sin \eta\tau)J_{11}\sin(x_2)\right],$$

$$\dot{x}_2 = x_3,$$

$$\dot{x}_3 = \frac{1}{A(x_2)}\left[\frac{1}{2}K(x_2)Z(x_2)x_1^2 + b(x_2)J(x_2)x_3^2 - b(x_2)\bar{k}_1x_1 - K(x_2)\bar{k}_2x_3 - b(x_2)Z(x_2)x_1x_3 \right.$$

$$\left. + K(x_2)(1 + \gamma \sin \eta\tau)J_{11}\sin(x_2)\right], \tag{14}$$

where $x_1 = \ddot{\alpha}$, $x_2 = \beta$ and $x_3 = \dot{\beta}$.

3. STABILITY ANALYSIS BY LYAPUNOV DIRECT METHOD

The stability in finite region of the solution of the rigid-body system is investigated by Lyapunov direct method in this section. There are two equilibrium points, $(0, \pi, 0)$, $(0, 0, 0)$ in equations (8) and (9).

First, consider the stability of the equilibrium point $(0, \pi, 0)$. Let $\dot{\alpha} = 0 + y_1$, $\beta = \pi + y_2$ and $\dot{\beta} = 0 + y_3$, where y_1, y_2, y_3 are small disturbances. Then, transform equations (8) and (9) above into the following state equations:

$$\dot{y}_1 = \frac{1}{A(\pi + y_2)}\left[\frac{1}{2}b(\pi + y_2)Z(\pi + y_2)y_1^2 + J_{11}J(\pi + y_2)y_3^2 - J_{11}k_1y_1 - b(\pi + y_2)k_2y_3 \right.$$

$$\left. - J_{11}Z(\pi + y_2)y_1y_3 + b(\pi + y_2)mg_0h\sin(\pi + y_2)\right],$$

$$\dot{y}_2 = y_3,$$

$$\dot{y}_3 = \frac{1}{A(\pi + y_2)}\left[\frac{1}{2}K(\pi + y_2)Z(\pi + y_2)y_1^2 + b(\pi + y_2)J(\pi + y_2)y_3^2 - b(\pi + y_2)k_1y_1 \right.$$

$$\left. - K(\pi + y_2)k_2y_3 - b(\pi + y_2)Z(\pi + y_2)y_1y_3 + K(\pi + y_2)mg_0h\sin(\pi + y_2)\right].$$

Expanding $\sin\beta$ and $\cos\beta$ as power series, the state equations become

$$\dot{y}_1 = -J_{11}k_1ay_1 + J_{13}mg_0hay_2 + J^{13}k_2ay_3 + , \ldots,$$

$$\dot{y}_2 = y_3,$$

$$\dot{y}_3 = J_{13}k_1ay_1 - J_{33}mg_0hay_2 - J_{33}k_2ay_3 + , \ldots,$$

where "$\cdots$" means higher order terms and

$$a = \frac{1}{J_{11}J_{33} - J_{33}^2}.$$

Construct Lyapunov function as

$$V(y_1, y_2, y_{32}) = \tfrac{1}{2}J_{33}y_1^2 + \tfrac{1}{2}mg_0hy_2^2 + \tfrac{1}{2}J_{11}y_3^2 + J_{13}y_1y_3.$$

By Sylvester's theorem, the sufficient condition for the positive definiteness of function $V(y_1, y_2, y_3)$ is

$$(J_{11}J_{33} - J_{33}^2) > 0.$$

The derivative $\dot{V}(y_1, y_2, y_3)$ is given by

$$\dot{V}(y_1, y_2, y_3) = -k_1y_1^2 - k_2y_3^2.$$

Thus, $\dot{V} \leqslant 0$ for all (y_1, y_2, y_3) and $\dot{V} = 0$ if and only if $y_1 = y_3 = 0$. We compute the higher order derivatives of V and find

$$\ddot{V} = -2k_1y_1\dot{y}_1 - 2k_2y_3\dot{y}_3 = 0,$$

when $y_1 = y_3 = 0$

$$\dddot{V} = -2(k_1J_{13}^2 + k_2J_{33}^2)(mg_0ha)^2y_2^2 < 0$$

when $y_2 \neq 0$.

From the sufficient conditions of the Mukherjee and Chen theorem [4], we can conclude the asymptotic stability of the equilibrium point $(0, \pi, 0)$ of this system.

The stability of the equilibrium point $(0, 0, 0)$ is also considered by Lyapunov direct method. Let $\dot{\alpha} = 0 + x_1$, $\beta = 0 + x_2$ and $\dot{\beta} = 0 + x_3$, where x_{12}, x_2, x_3 are small disturbances. Then, transform equations (8) and (9) into the following state equations:

$$\dot{x}_1 = \frac{1}{A(x_2)}\left[\frac{1}{2}b(x_2)Z(x_2)x_1^2 + J_{11}J(x_2)x_3^2 - J_{11}k_1x_1 - b(x_2)k_2x_3 - J_{11}Z(x_2)x_1x_3 + b(x_2)mg_0h\sin(x_2)\right],$$

$$\dot{x}_2 = x_3,$$

$$\dot{x}_3 = \frac{1}{A(x_2)}\left[\frac{1}{2}K(x_2)Z(x_2)x_1^2 + b(x_2)J(x_2)x_3^2 - b(x_2)k_1x_1 - K(x_2)k_2x_3 - b(x_2)Z(x_2)x_1x_3 + K(x_2)mg_0h\sin(x_2)\right].$$

Expanding $\sin\beta$ and $\cos\beta$ as power series, the state equations becomes

$$\dot{x}_1 = -J_{11}k_1ax_1 + J_{13}mg_0hax_2 - J_{13}k_2ax_3 + , \ldots,$$

$$\dot{x}_2 = x_3,$$

$$\dot{x}_3 = -J_{13}k_1ax_1 + J_{33}mg_0hax_2 - J_{33}k_2ax_3 + , \ldots,$$

where "$\cdots$" means higher order terms and

$$a = \frac{1}{J_{11}J_{33} - J_{13}^2}.$$

Construct Lyapunov function as

$$V(x_1, x_2, x_3) = -\tfrac{1}{2}J_{33}x_1^2 + \tfrac{1}{2}mg_0hx_2^2 - \tfrac{1}{2}J_{11}x_3^2 + J_{13}x_1x_3.$$

The derivative $\dot{V}(x_1, x_2, x_3)$ is given by

$$\dot{V}(x_1, x_2, x_3) = k_1x_1^2 + k_2x_3^2.$$

Thus, $\dot{V} > 0$ for all x_1, x_2, x_3 and $\dot{V} = 0$ if and only if $x_1 = x_3 = 0$. We compute the higher order derivatives of V and find

$$\ddot{V} = 2k_1x_1\dot{x}_1 + 2k_2x_3\dot{x}_3 = 0,$$

where $x_1 = x_3 = 0$

$$\dddot{V} = 2(k_1J_{13}^2 + k_2J_{33}^2)(mg_0ha)^2x_2^2 > 0$$

for $x_2 \neq 0$. Also $V(0) = 0$.

From the sufficient conditions of a new theorem recently developed [5], we can conclude that the equilibrium point $(0, 0, 0)$ of this system is unstable.

4. BIFURCATION DIAGRAM AND LYAPUNOV EXPONENT

The bifurcation diagrams of the non-linear system of equation (14) are depicted in Figures 2 and 3. Numerical simulation has been carried out with the following set of parameter values: $J_{11} = 0{\cdot}4$, $J_{12} = 0{\cdot}11$, $J_{13} = 0{\cdot}13$, $J_{22} = 0{\cdot}37$, $J_{23} = 0{\cdot}12$, $J_{33} = 0{\cdot}35$, $\bar{k}_1 = 0{\cdot}15$, $\bar{k}_2 = 0{\cdot}15$ and $\eta = 0{\cdot}12$. They are plotted against the amplitude of the vibrating

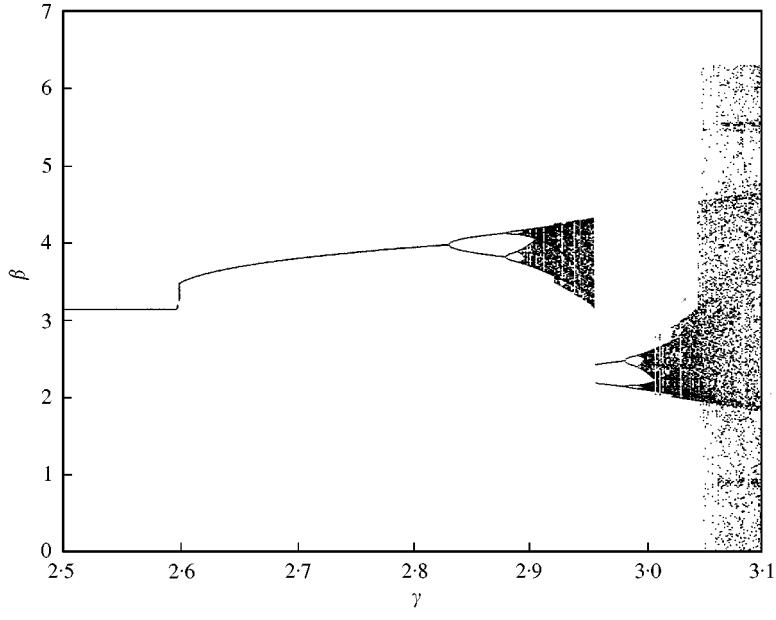

Figure 2. Bifurcation diagram γ versus β for one attractor.

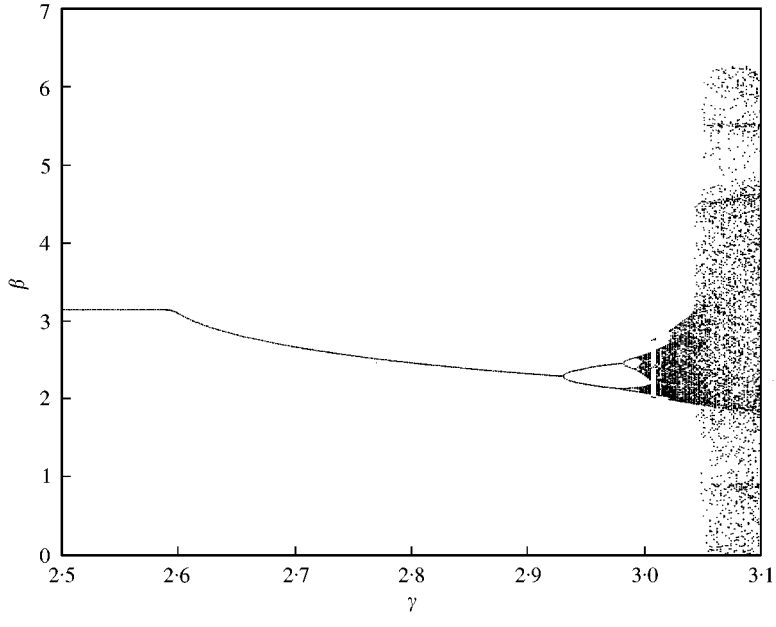

Figure 3. Bifurcation diagram γ versus β for another attractor.

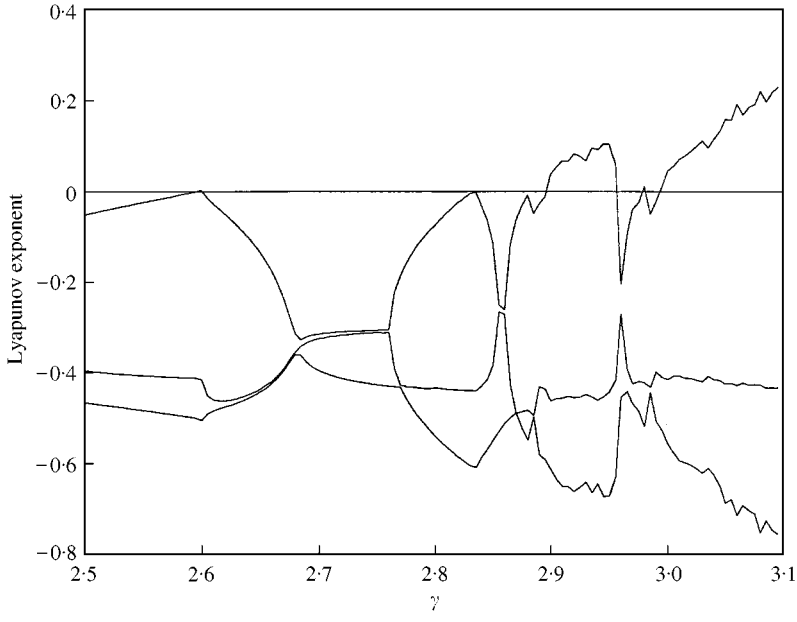

Figure 4. Lyapunov exponents for γ between 2·5 and 3·1 for attractor shown in Figure 2.

acceleration $\gamma \in [2{\cdot}5, 3{\cdot}1]$. It is worth mentioning that there are two different attractors as the parameter γ varied. Figures 2 and 3 present two different bifurcation diagrams for two different initial conditions. Periodic-doubling routes to chaos of our system will be shown by the bifurcation diagram.

The Lyapunov exponent calculation algorithm can serve as criteria for detecting the chaotic motion: a system is chaotic when there exists at least one positive Lyapunov exponent [6]. The signs of the Lyapunov exponents provide a qualitative picture of a system dynamics. The criterion is

$$\lambda > 0 \text{ (chaotic)}, \qquad \lambda \leqslant 0 \text{ (regular motion)}.$$

The Lyapunov exponents of the solutions of this non-linear dynamical system are plotted in Figures 4 and 5. It can be compared with bifurcation diagrams, Figures 2 and 3, for the two attractors.

5. PHASE PORTRAITS, POINCARÉ MAP AND POWER SPECTRUM ANALYSIS

A valuable description of a solution is obtained by examining its behaviour in the phase plane. When the solution becomes stable, the asymptotic behaviors of the phase trajectories are of particular interest and the transient behaviors in the system are neglected. The Poincaré map is a method which can simplify phase portrait of complicate systems. The phase portraits and Poincaré map are shown in Figures 6 and 7 for two attractors respectively.

The power spectrum analysis of the non-linear dynamical system, equation (14), are shown in Figure 8 for $\gamma = 3{\cdot}03$. The noise-like spectrum, in Figure 8, is characteristic of chaotic dynamical system. The chaotic spectrum is a continuous broadband one. Although

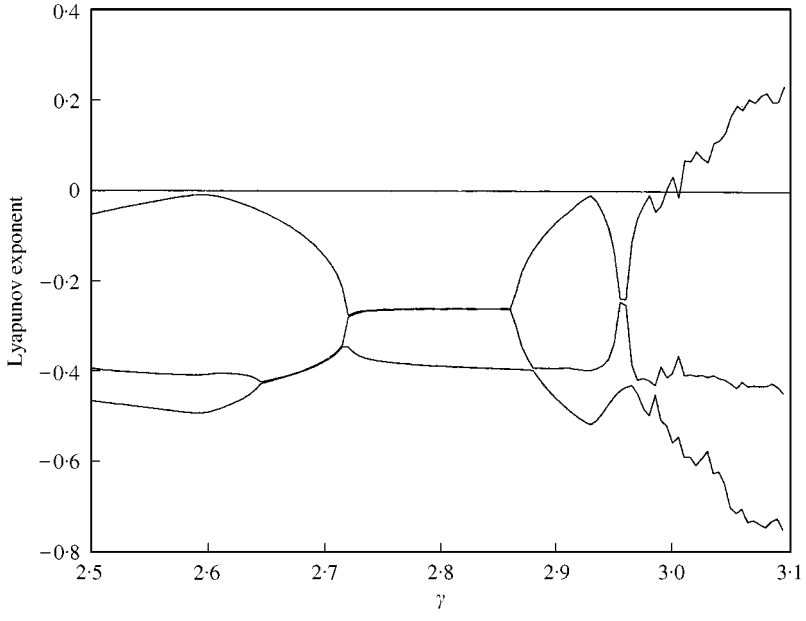

Figure 5. Lyapunov exponents for γ between 2·5 and 3·1 for attractor shown in Figure 3.

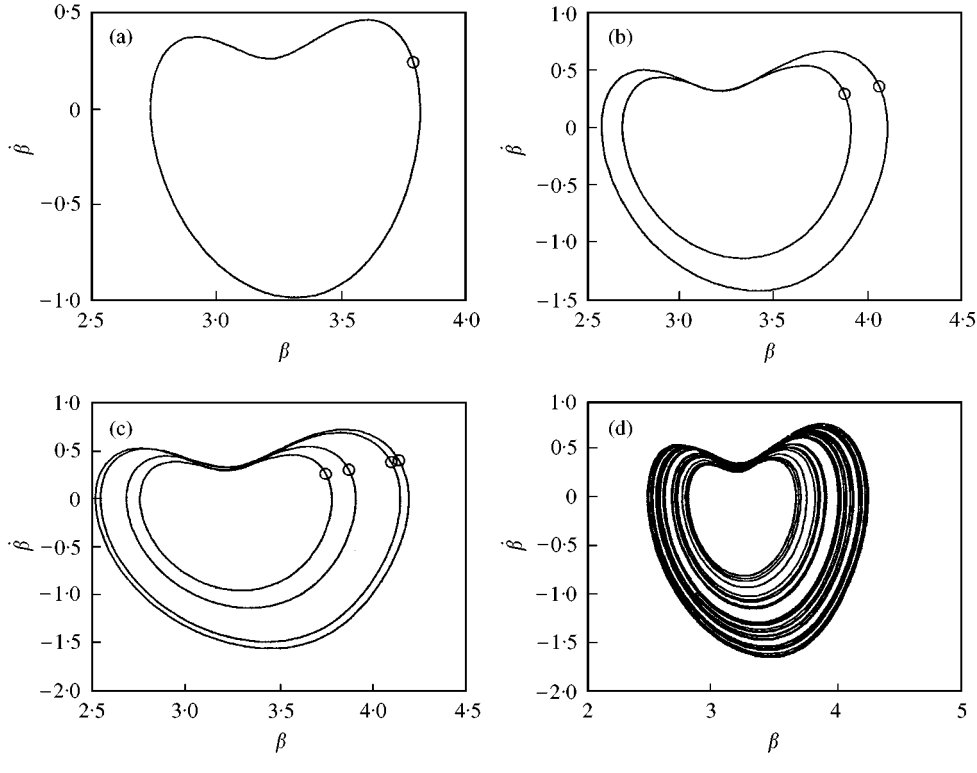

Figure 6. Poincaré maps and phase portraits for attractor shown in Figure 2. (a) 1T, (b) 2T, (c) 4T, (d) chaos.

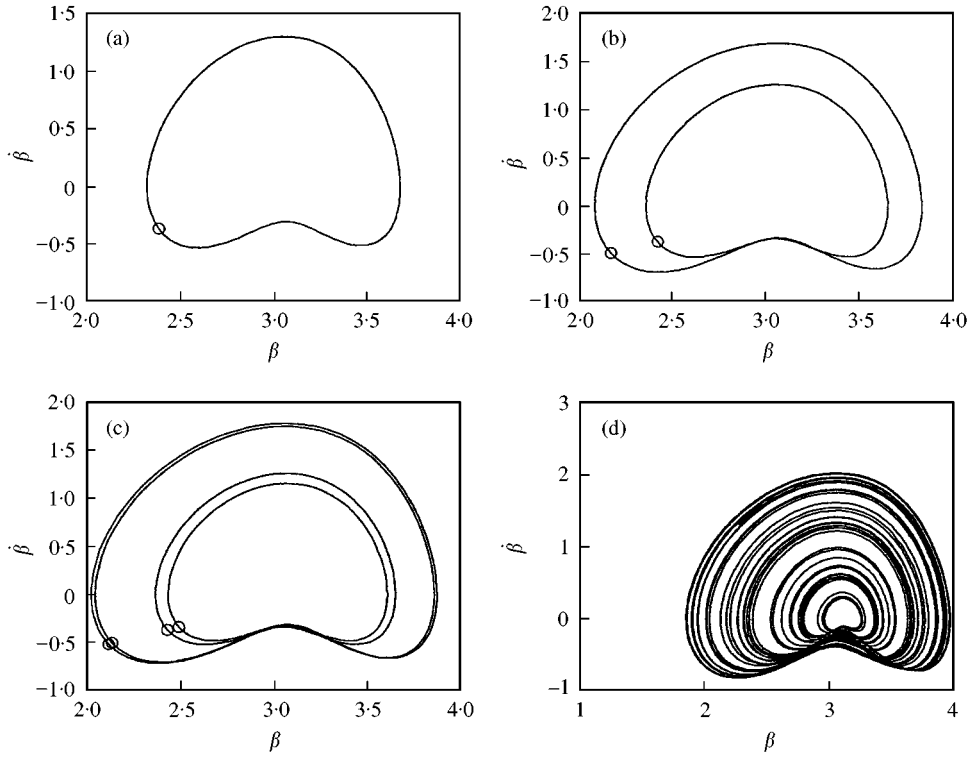

Figure 7. Poincaré maps and phase portraits for attractor shown in Figure 3. (a) 1T, (b) 2T, (c) 4T, (d) chaos.

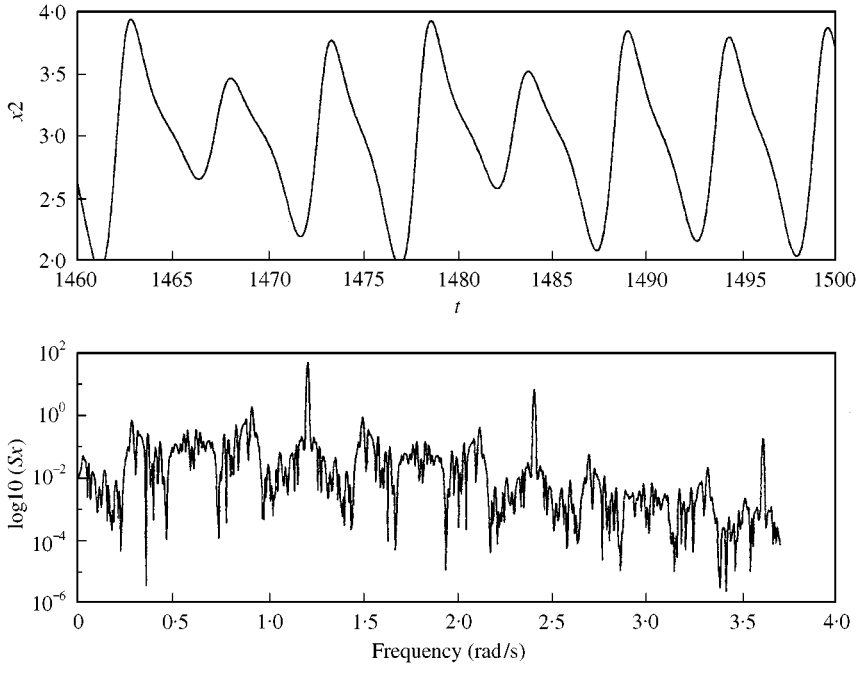

Figure 8. Time history and power spectrum for $\gamma = 3{\cdot}03$.

a broadband spectrum does not guarantee sensitivity to initial conditions, it is still a reliable indicator of chaos.

6. INCREMENTAL HARMONIC BALANCE METHOD

The IHB method is a combination of the incremental method with the harmonic balance method. The steady state periodic solutions of equation (14) are obtained by the IHB method, which can deal with strong non-linearity very well and is convenient for computer implementation [7–10].

From equations (12) and (13), let $\tau_1 = \Omega\tau$, the equations become

$$\Omega^2\dot{x}_1 = \frac{1}{A(x_2)}\left[\frac{1}{2}b(x_2)Z(x_2)\Omega^2x_1^2 + J_{11}J(x_2)\Omega^2x_3^2 - J_{11}k_1\Omega x_1 - b(x_2)k_2\Omega x_3 \right.$$
$$\left. - J_{11}Z(x_2)\Omega^2x_1x_3 + b(x_2)(1+\gamma\sin\tau)J_{11}\sin(x_2)\right]$$

$$\dot{x}_2 = x_3,$$

$$\Omega^2\dot{x}_3 = \frac{1}{A(x_2)}\left[\frac{1}{2}K(x_2)Z(x_2)\Omega^2x_1^2 + b(x_2)J(x_2)\Omega^2x_3^2 - b(x_2)k_1\Omega x_1 - K(x_2)k_2\Omega x_3 \right.$$
$$\left. - b(x_3)Z(x_2)\Omega^2x_1x_3 + K(x_2)(1+\gamma\sin\tau)J_{11}\sin(x_2)\right]. \tag{15}$$

The first step of the IHB method is a Newton–Raphson procedure. Let $\Omega_0, x_{10}, x_{20}, x_{30}$ and γ_0 be a solution, the neighbouring state can be expressed by adding the corresponding increments to them as follows:

$$x_1 = x_{10} + \Delta x_1, \quad x_2 = x_{20} + \Delta x_2, \quad x_3 = x_{30} + \Delta x_3,$$
$$\gamma = \gamma_0 + \Delta\gamma, \quad \Omega = \Omega_0 + \Delta\Omega. \tag{16}$$

Substituting equation (16) into equation (15) and neglecting the small terms of higher order, the linearized incremental equation can be derived as

$$A(x_{20})\Omega_0^2\Delta\dot{x}_1 + (M_1 + J_{11}k_1\Omega_0)\Delta x_1 + M_2\Delta x_2 + M_3\Delta x_3 = M_4\Delta\Omega + M_5\Delta\gamma + M_6,$$

$$\Delta\dot{x}_2 - \Delta x_3 = x_{30} - \dot{x}_{20},$$

$$A(x_{20})\Omega_0^2\Delta\dot{x}_3 + M_7\Delta x_1 + M_8\Delta x_2 + M_9\Delta x_3 = M_{10}\Delta\Omega + M_{11}\Delta\gamma + M_{12}. \tag{17}$$

For convenience, equation (17) can be rewritten in matrix form as

$$G\Delta\dot{\mathbf{X}} + \mathbf{K}\Delta\mathbf{X} = \mathbf{R} + \mathbf{F}\Delta\Omega + \mathbf{D}_1\Delta\gamma, \tag{18}$$

where $\Delta\mathbf{X} = [\Delta x_1\ \Delta x_2\ \Delta x_3]^{\mathrm{T}}$ and $M_1, M_2, M_3, M_4, M_5, M_6, M_7, M_8, M_9, M_{10}, M_{11}, M_{12}$, **G, K, R, F, D$_1$** are given in Appendix A. The corrective vector **R** in equation (18) plays an

important role. It prevents the incrementation process drifting from the exact solution. The corrective term **R** goes to zero when the solution is reached. Since one is primarily interested in the phase portraits of the system for a constant frequency and the amplitude of the vibrating acceleration, γ and Ω are fixed as a parameter vector, which imply $\Delta\gamma = \Delta\Omega = 0$. Hence, equation (18) is reduced to

$$\mathbf{G}\Delta\dot{\mathbf{X}} + \mathbf{K}\Delta\mathbf{X} = \mathbf{R}. \tag{19}$$

The second step of the IHB method is Galerkin's procedure. For steady state response, an approximate periodic solution may be assumed as

$$\mathbf{x}_1 = \sum_{j=0}^{N}\left(a_j \cos\frac{j}{q}\tau_I + b_j \sin\frac{j}{q}\tau_I\right) = \mathbf{D}\mathbf{A},$$

$$\Delta x_1 = \sum_{j=0}^{N}\left(\Delta a_j \cos\frac{j}{q}\tau_I + \Delta b_j \sin\frac{j}{q}\tau_I\right) = \mathbf{D}\Delta\mathbf{A},$$

$$x_2 = \sum_{j=0}^{N}\left(c_j \cos\frac{j}{q}\tau_I + d_j \sin\frac{j}{q}\tau_I\right) = \mathbf{D}\mathbf{B},$$

$$\Delta x_2 = \sum_{j=0}^{N}\left(\Delta c_j \cos\frac{j}{q}\tau_I + \Delta d_j \sin\frac{j}{q}\tau_I\right) = \mathbf{D}\Delta\mathbf{B},$$

$$x_3 = \sum_{j=0}^{N}\left(e_j \cos\frac{j}{q}\tau_I + f_j \sin\frac{j}{q}\tau_I\right) = \mathbf{D}\mathbf{C},$$

$$\Delta x_3 = \sum_{j=0}^{N}\left(\Delta e_j \cos\frac{j}{q}\tau_I + \Delta f_j \sin\frac{j}{q}\tau_I\right) = \mathbf{D}\Delta\mathbf{C},$$

where **D, A,** Δ**A, B,** Δ**B, C** and Δ**C** are given in Appendix A.

Hence, the vectors of unknown solutions and their increments can be written as

$$\mathbf{X}_0 = \mathbf{P}\mathbf{Q}, \qquad \Delta\mathbf{X} = \mathbf{P}\Delta\mathbf{Q}, \tag{20, 21}$$

where

$$\mathbf{P} = \begin{bmatrix} \mathbf{D} & 0 & 0 \\ 0 & \mathbf{D} & 0 \\ 0 & 0 & \mathbf{D} \end{bmatrix}, \quad \mathbf{Q} = [\mathbf{A} \quad \mathbf{B} \quad \mathbf{C}]^{\mathrm{T}} \quad \text{and} \quad \Delta\mathbf{Q} = [\Delta\mathbf{A}\ \Delta\mathbf{B}\ \Delta\mathbf{C}]^{\mathrm{T}}.$$

Putting equations (20) and (21) into equation (19), and applying the Galerkin procedure, we have

$$\delta\Delta\mathbf{Q}^{\mathrm{T}}\left\{\int_0^{2\pi}\mathbf{P}^{\mathrm{T}}[\mathbf{G}\dot{\mathbf{P}} + \mathbf{K}\mathbf{P}]\,\mathrm{d}\tau\right\}\Delta\mathbf{Q} = \delta\Delta\mathbf{Q}^{\mathrm{T}}\left\{\int_0^{2\pi}\mathbf{P}^{\mathrm{T}}\mathbf{R}\,\mathrm{d}\tau\right\} \tag{22}$$

or simplify

$$\mathbf{M}\Delta\mathbf{Q} = \bar{\mathbf{R}}, \tag{23}$$

where **M** and $\bar{\mathbf{R}}$ are given in Appendix A.

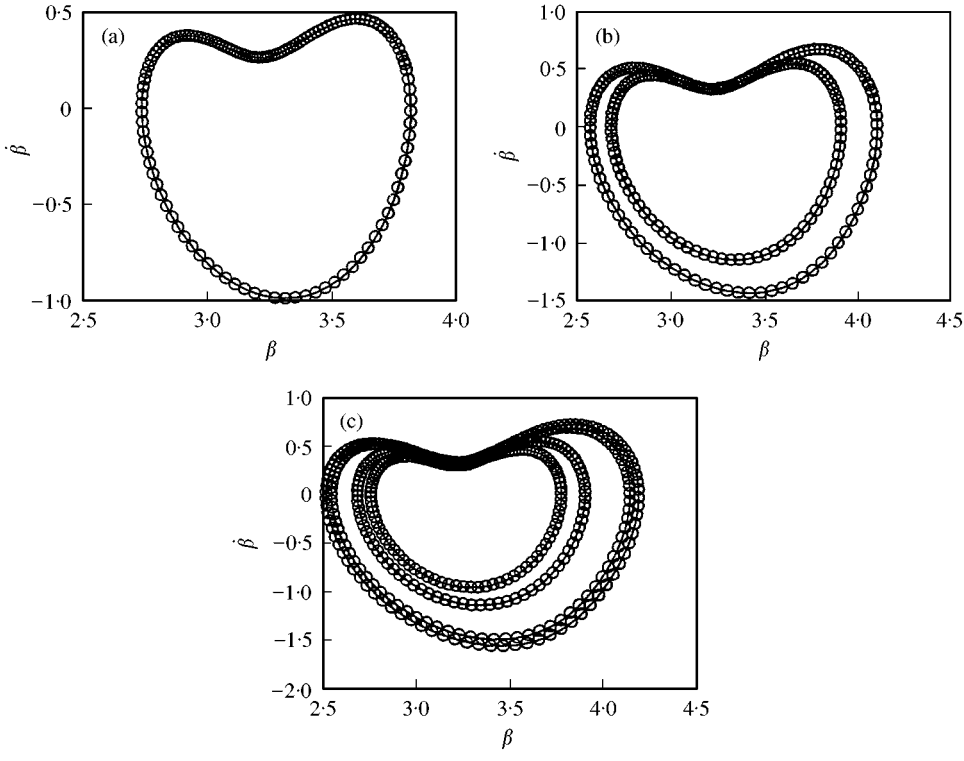

Figure 9. The solutions of IHB: (a) 1T, (b) 2T, (c) 4T. Compare with Figure 6.

An initial solution should first be given in the process of solving equation (19). At every iteration process, we proceed to solve this equation until the following criterion is satisfied:

$$\| \bar{\mathbf{R}} \| \leqslant \varepsilon,$$

where $\| \bar{\mathbf{R}} \|$ is the magnitude of the corrective vector $\bar{\mathbf{R}}$ and ε is the tolerance depending on the accuracy required.

The phase portraits obtained by the IHB method in comparison with those obtained by numerical integration are shown in Figures 9(a)–9(c) and 10(a)–10(c), in which the symbol "o" indicates the solution obtained by IHB. These solutions are in good agreement. The bifurcation diagrams by IHB method are shown in Figures 11 and 12 which can be compared with Figures 2 and 3.

7. MODIFIED INTERPOLATED CELL MAPPING METHOD

It is well known that different initial conditions may lead to different attractors when the governing differential equations are non-linear. Hence, finding a method to determine which solution will occur for a given initial condition is the major task. The attractors and corresponding basins of attraction of the system can be found by the modified interpolated cell mapping method (MICM) [11], which improved from interpolated cell mapping method [12].

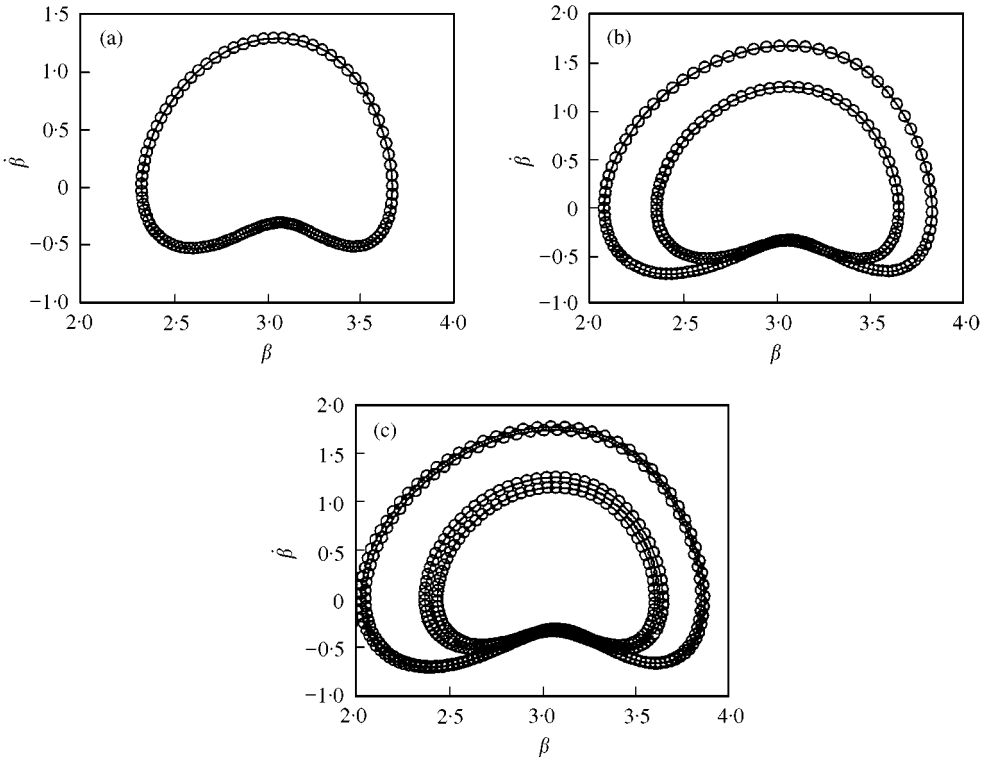

Figure 10. The solutions of IHB: (a) 1T, (b) 2T, (c) 4T. Compare with Figure 7.

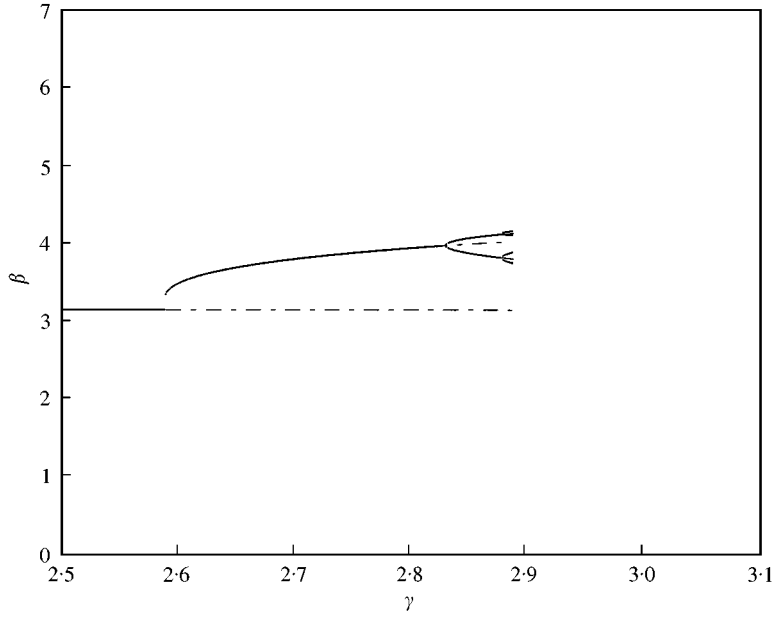

Figure 11. Bifurcation diagram by IHB method. Compare with Figure 2.

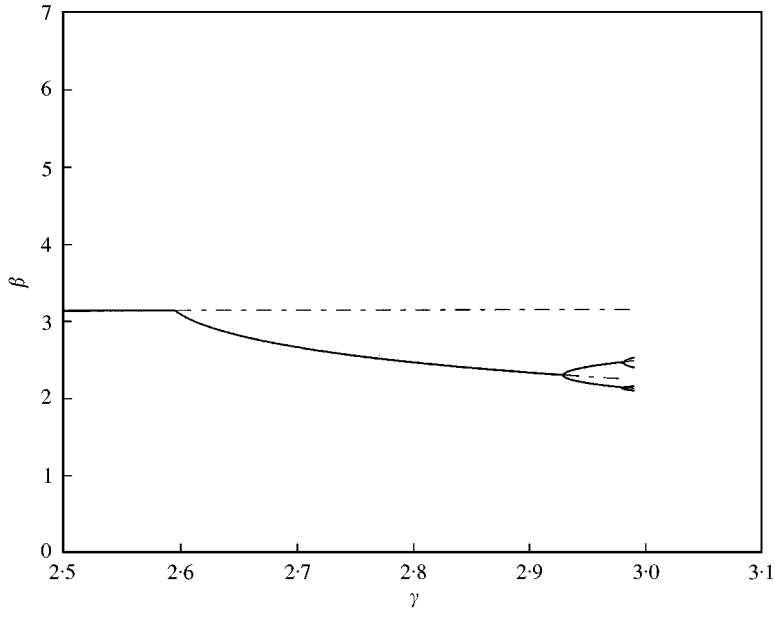

Figure 12. Bifurcation diagram by IHB method. Compare with Figure 3.

For three-dimensional system, 303^3 cells are studied by modified interpolated mapping method, where 303 is the number of the total cells divided in each dimensional region of interest. The mapping function is a 27818 127 ($303 \times 303 \times 303$) grid of points distributed in phase plane by using Runge–Kutta integration algorithm. As the distance between two trajectories is less than 10^{-5}, it is considered to be periodic.

The results of this dynamical system by the method MICM are depicted in Figures 13–16 respectively. In Figure 13(a), two black dots for $\gamma = 2{\cdot}7$ indicate that the system has two attractors and both are period-1T motion. There are three sections, $X_1 = -2$, 0 and 2, for the corresponding basins of attraction are shown in Figure 13. The symbols "·" (gray area) and "×" (black area) denote the cells attracted by different attractors. If initial conditions locate at gray area in Figure 13, then this system will tend to the left-side attractor, and the initial conditions in black area will tend to the right-side attractor. Figures 14–16 show the phenomena for $\gamma = 2{\cdot}85$, 2·89 and 2·91, respectively, and the initial conditions in gray area always tend to the left-side attractor (period-1T).

The special phenomena is called fractal, and the boundary is called fractal basin boundary. In order to observe it, the structure of the fractal basin boundary is enlarged in Figures 17(a)and 17(b). Hence, small uncertainties in initial conditions or other system parameters may lead to uncertainties in the consequence of the state of the non-linear system.

8. CONTROLLING OF CHAOS BY ADDITION OF A CONSTANT TORQUE

One can even add just a constant torque to control the chaotic behavior to a desired periodic one in a typical non-linear system. It ensures effective controlling in a very simple ways. Examining the effect of the constant torque, the added torque is assumed to be present in equations (12) and (13). Equations (12) and (13) with the constant torque γ_2 can be

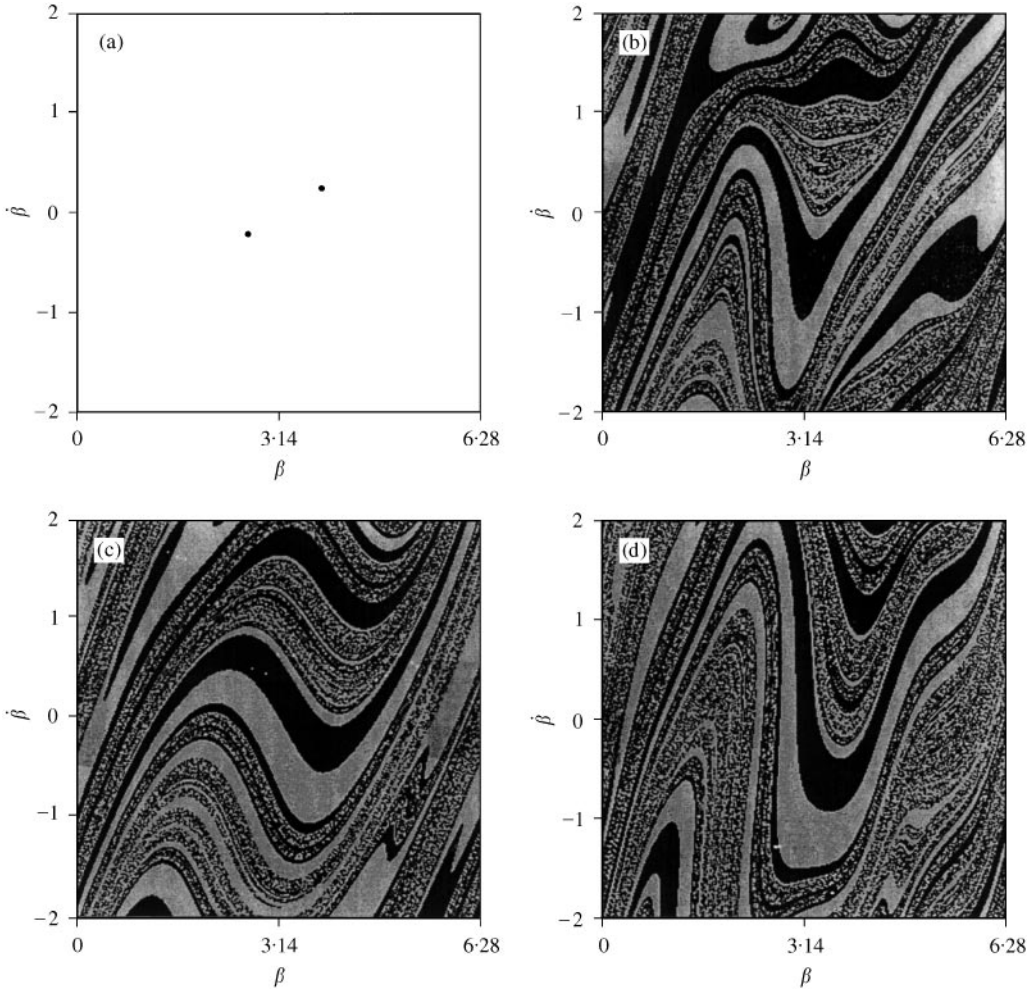

Figure 13. (a) The projection of attractors. (b)–(d) Basins of attraction for $\gamma = 2{\cdot}7$, $\alpha = -2, 0, 2$.

written as

$$\ddot{\alpha} - \frac{b(\beta)}{K(\beta)}\ddot{\beta} + \frac{Z(\beta)}{K(\beta)}\dot{\alpha}\dot{\beta} - \frac{J(\beta)}{K(\beta)}\dot{\beta}^2 + \frac{\bar{k}_1}{K(\beta)}\dot{\alpha} = 0,$$

$$\ddot{\beta} - \frac{b(\beta)}{J_{11}}\ddot{\alpha} - \frac{1}{2}\frac{Z(\beta)}{J_{11}}\dot{\alpha}^2 - (1 + \gamma \sin \eta\tau)\sin\beta + \frac{\bar{k}_2}{J_{11}}\dot{\beta} + \gamma_2 = 0.$$

Consider the effect of the constant torque by increasing it from zero upwards, the chaotic behavior is modified. By using Lyapunov exponents, the parameter that can stabilize the motion of this system can be found. In Figures 18(a) and 18(b), the maximal Lyapunov exponents are shown for $\gamma = 2{\cdot}91$ and $3{\cdot}1$. When the constant torque γ_2 is present at certain intervals, the maximal Lyapunov exponents $\lambda_i \leqslant 0$, it is clear that the system returns to regular behavior.

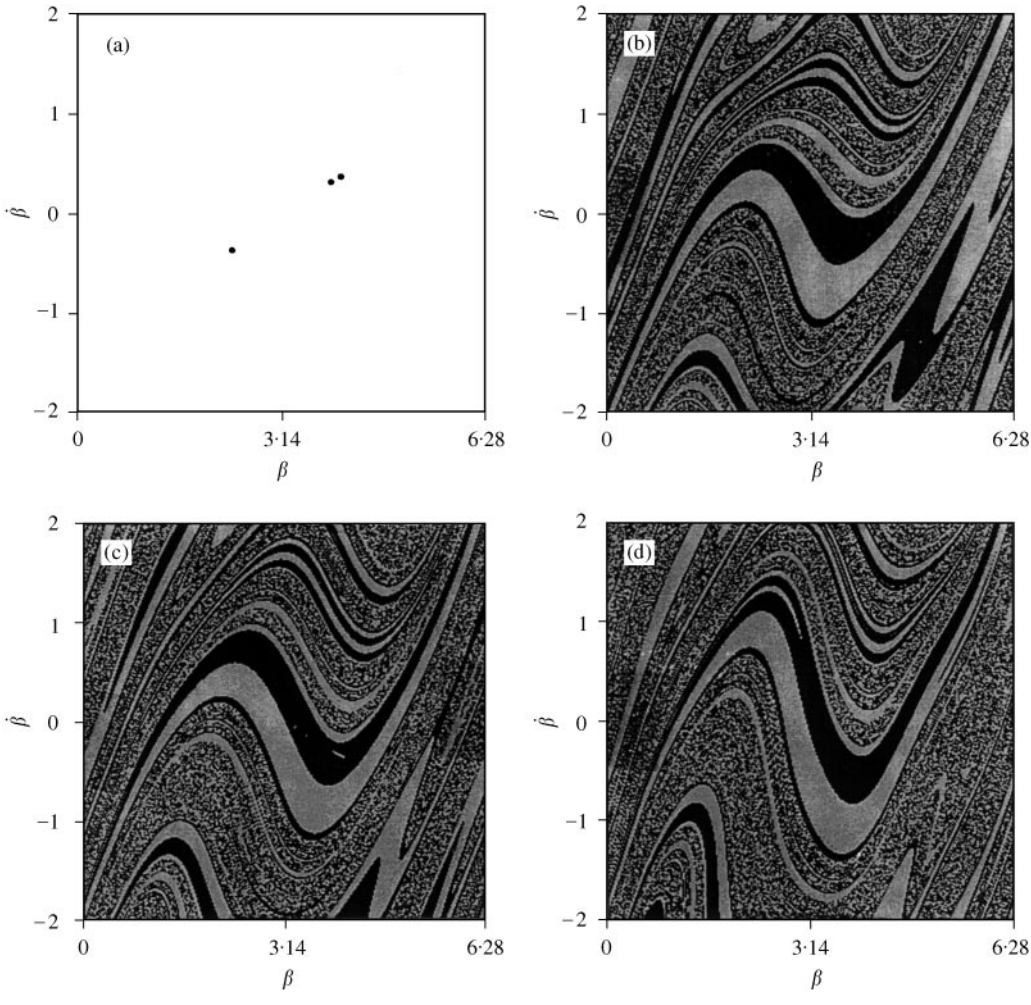

Figure 14. (a) The projection of attractors. (b)–(d) Basins of attraction for $\gamma = 2{\cdot}85$, $\alpha = -1, 0, 1$.

9. CONTROLLING OF CHAOS BY ADDITION OF A PERIODIC TORQUE

One can also control system dynamics by the addition of the external periodic torque in the chaotic state [13]. Equations (12) and (13) with the second periodic torque $\gamma_2 \sin \Omega\tau$ can be written as

$$\ddot{\alpha} - \frac{b(\beta)}{K(\beta)}\ddot{\beta} + \frac{Z(\beta)}{K(\beta)}\dot{\alpha}\dot{\beta} - \frac{J(\beta)}{K(\beta)}\dot{\beta}^2 + \frac{\bar{k}_1}{K(\beta)}\dot{\alpha} = 0,$$

$$\ddot{\beta} - \frac{b(\beta)}{J_{11}}\ddot{\alpha} - \frac{1}{2}\frac{Z(\beta)}{J_{11}}\dot{\alpha}^2 - (1 + \gamma \sin \eta\tau)\sin\beta + \frac{\bar{k}_2}{J_{11}}\dot{\beta} + \gamma_2 \sin \Omega\tau = 0.$$

When $\gamma_2 \in [0,\ 0{\cdot}1]$, $\Omega = \eta$ and $\gamma = 2{\cdot}91$, detailed structure of maximal Lyapunov exponent against γ_2 is shown in Figure 19(a). When $\gamma_2 \in [0, 1]$, $\Omega \neq \eta$ and $\gamma = 3{\cdot}03$, detailed

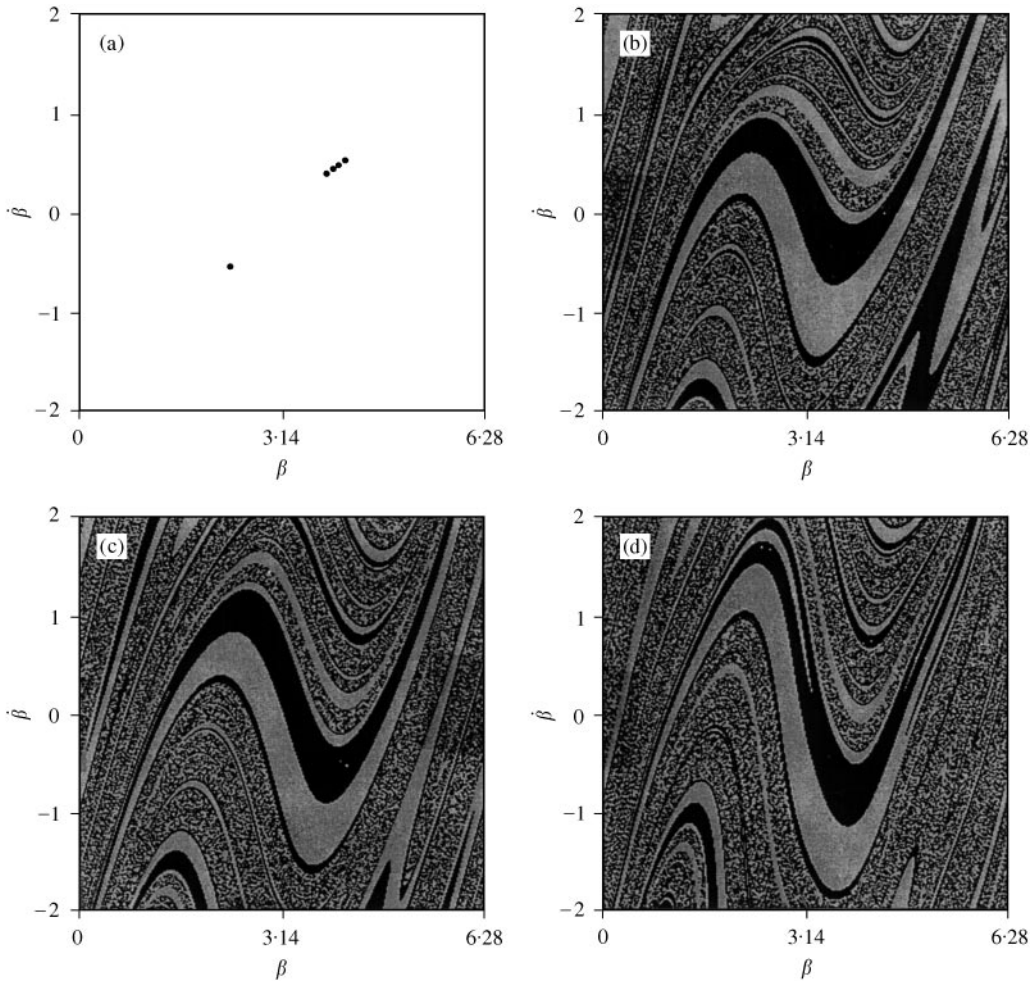

Figure 15. (a) The projection of attractors. (b)–(d) Basins of attraction for $\gamma = 2{\cdot}89$, $\alpha = -1, 0, 1$.

structure of maximal Lyapunov exponent versus γ_2 is shown in Figure19(b). When the maximal Lyapunov exponents $\lambda_i \leqslant 0$, it is clear that the system returns to regular behavior.

10. CONTROLLING OF CHAOS BY ADDITION OF DIETHER SIGNALS

In this section, we show that injecting another external input, called a dither signal, into this chaotic system, just ahead of non-linearity can control the chaos behavior [14]. Using the dither signal method, we can convert the chaotic motion to a periodic orbit or a steady state dependent on the system input. This approach is somewhat different from the weak periodic perturbation method, in which the control parameters (amplitude and frequency) of the external periodic torque must be adjusted, usually by trial and error. In experimental situations, if the location of the non-linearity is known, but the system parameters are unknown and unalterable, only the amplitude of dither signal needs to be tuned.

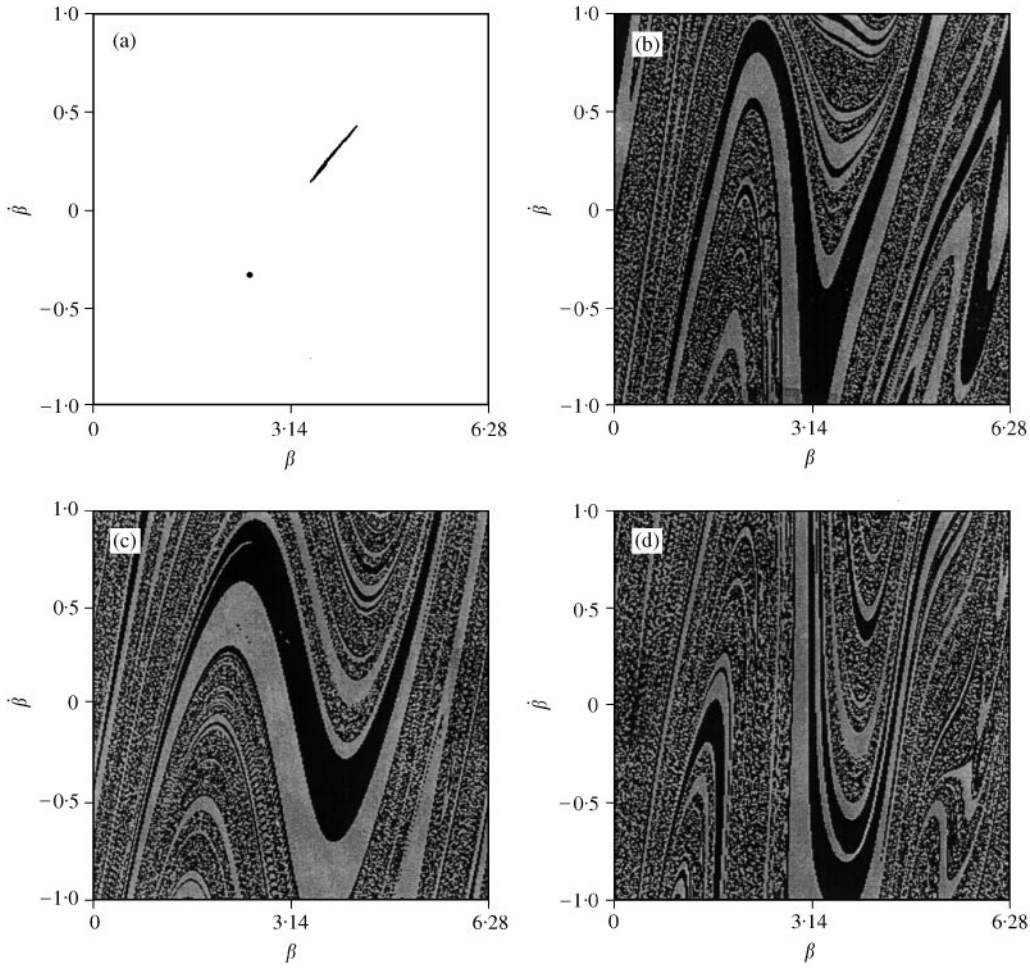

Figure 16. (a) The projection of attractors. (b)–(d) Basins of attraction for $\gamma = 2{\cdot}91$, $\alpha = -2, 0, 2$.

For this system, let us add a square-wave dither, whose frequency and amplitude are 2000 and 0·2, respectively, in the chaotic system after 100 s. The results are shown in Figure 20 for $\gamma = 3{\cdot}03$. The dynamics convert chaotic behavior to periodic motion, as shown in Figure 20(a). Figure 20(b) and 20(c) shows the phase portrait before and after control of the system. The drawback of this method is that the response after control is tuned by trial and error.

11. DELAYED FEEDBACK CONTROL

Let us consider a feedback structure employing a delayed copy of the output signal [15, 16]. The control signal applied to this system is proportional to the difference between the output and a delayed copy of the same output:

$$F(\tau) = K[y(\tau) - y(\tau - \tau_d)].$$

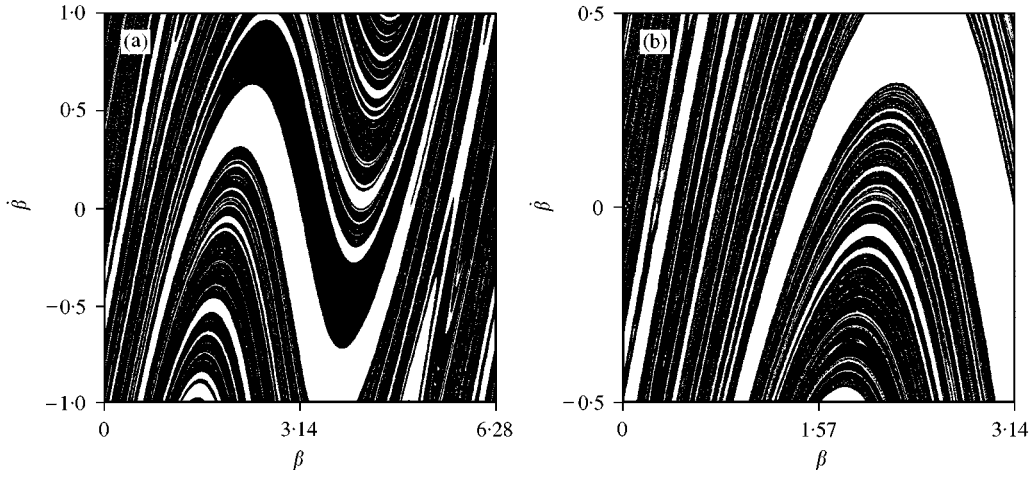

Figure 17. (a)–(b) Fractal-like basin of attractor for $\gamma = 2{\cdot}91$.

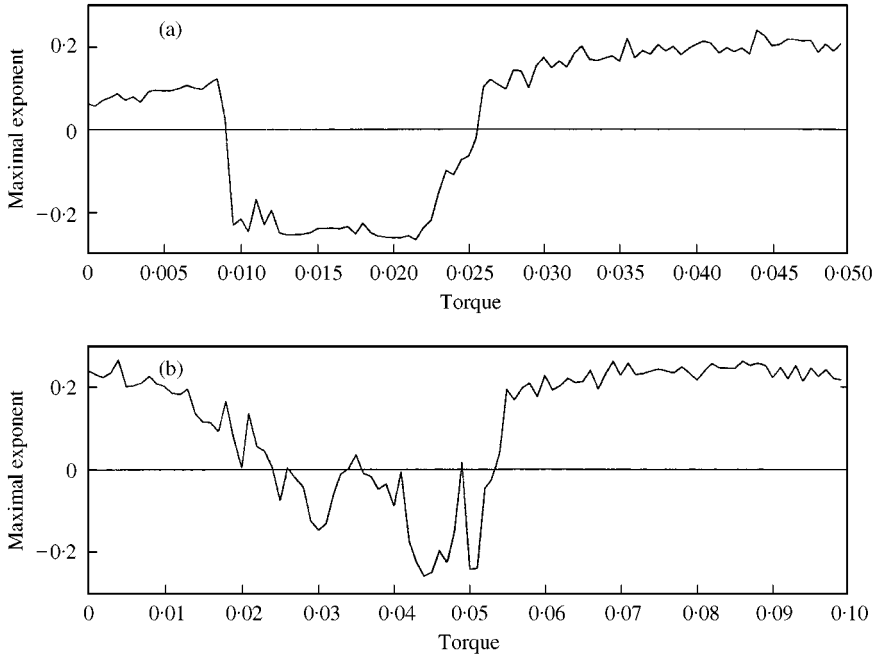

Figure 18. The maximal Lyapunov exponent for (a) $\gamma = 2{\cdot}91$, (b) $\gamma = 3{\cdot}1$ by addition of constant torque.

Depending on the delay constant τ_d and linear factor K, various kinds of periodic behaviors can be observed in the chaotic system. The result, when $\gamma = 2{\cdot}91$, is shown in Figures 21(a), 21(b), 21(c) and 21(d) for chaos, 1T, 2T and 4T respectively.

The positive features of the delay feedback control method are, first, self-control (no external signals are injected), and second, that no access to system parameters is required. The primary drawback of this method is that there is no *a priori* knowledge of the goal (the goal is accomplished by trial and error).

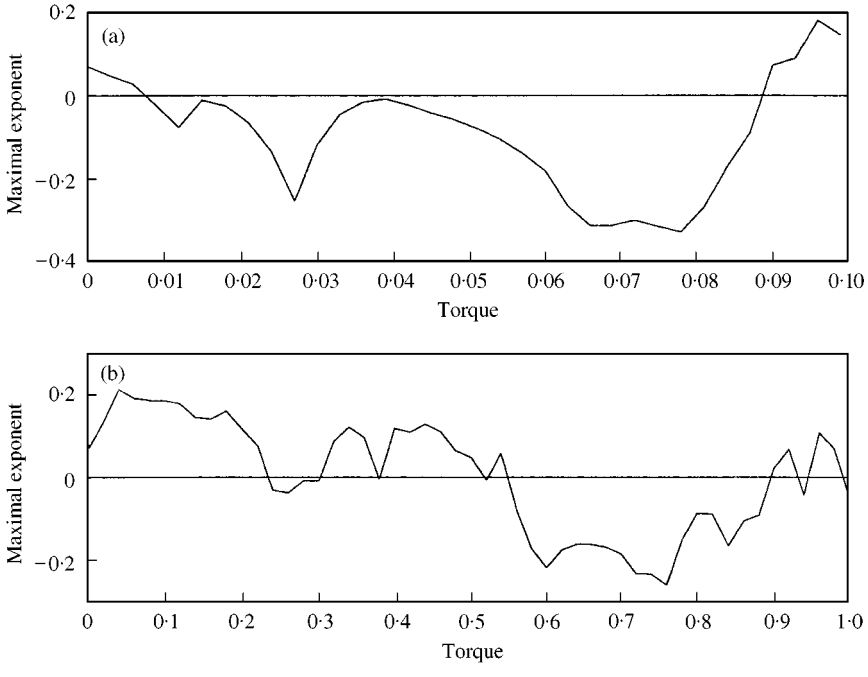

Figure 19. (a) The Lyapunov exponent for $\gamma = 2{\cdot}91$, $\Omega = \eta$ by the addition of periodic torque. (b) The Lyapunov exponent for $\gamma = 3{\cdot}03$, $\Omega \neq \eta$ by the addition of periodic torque.

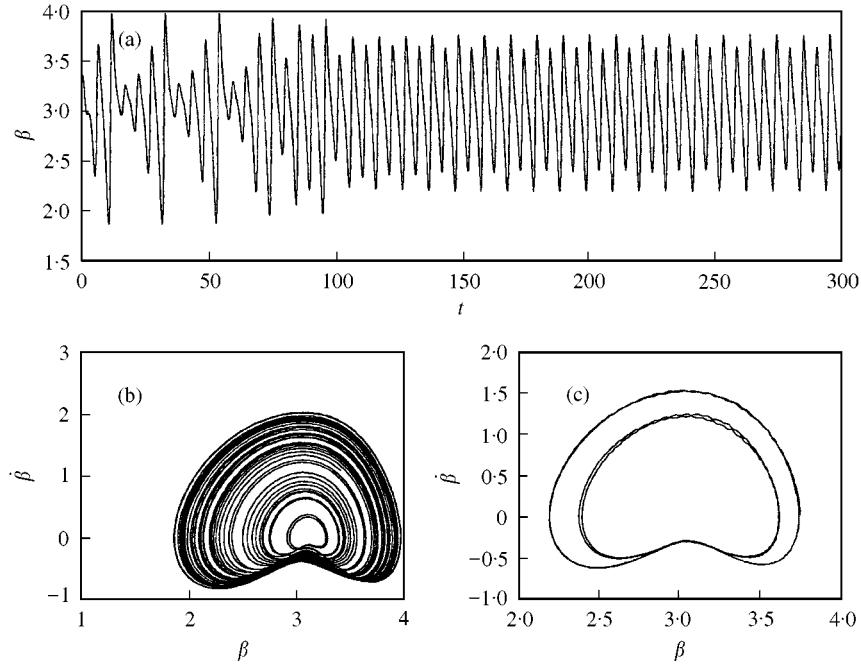

Figure 20. (a) Time history for $\gamma = 3{\cdot}03$ by the addition of dither signals; (b) phase portrait for uncontrolled system; (c) phase portrait for controlled system.

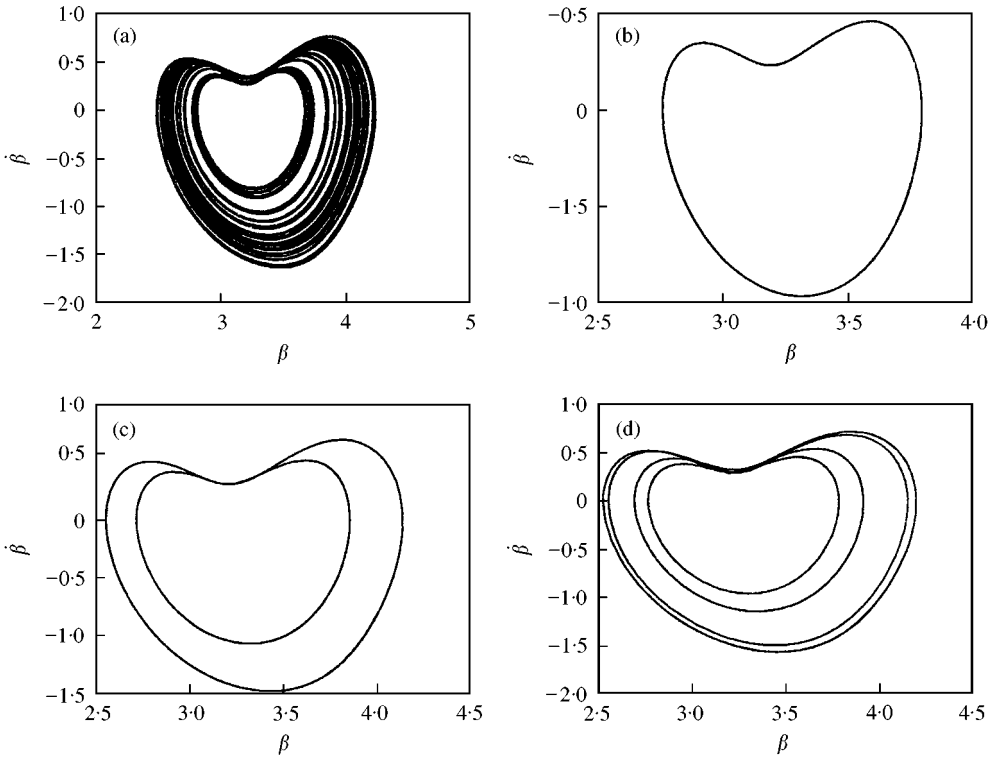

Figure 21. (a)–(d) Phase portraits of delayed feedback control for $\gamma = 2{\cdot}91$.

12. ADAPTIVE CONTROL

An adaptive control algorithm can be extended to multi-parameter and higher-dimensional non-linear system [17]. This control law is remarkably effective in returning a system to its original periodic solution by a perturbation in the system parameter changes of the dynamical behavior. A simple and effective adaptive control algorithm has been suggested, which utilizes an error signal proportional to the difference between the desired output and the actual output of the system. This error signal governs the change of the parameter of the system, which readjusts so as to reduce the error to zero. For a general N-dimensional dynamical system

$$\dot{X} \equiv \frac{\mathrm{d}X}{\mathrm{d}\tau} = F(X, \tau, \mu),$$

where $X \equiv (X_1, X_2, \ldots, X_N)$ are variable and $\mu \equiv (\mu_1, \mu_2, \ldots, \mu_M)$ are parameters, which determine the nature of the dynamics; the prescription for effective adaptive control is through the additional dynamics,

$$\dot{\mu} = \varepsilon G(X - X_s),$$

where X_s is the desired steady state value, ε indicates the stiffness of control and $G(X - X_s)$ is some suitable function with $G(0) = 0$. It is important whether the control algorithm is sensitive to the specific forms of the control dynamics, namely the choice for the function G. In some situation, we can try $G = y^2, y^{1/2}, \sin y$ and $y(1 - y)$.

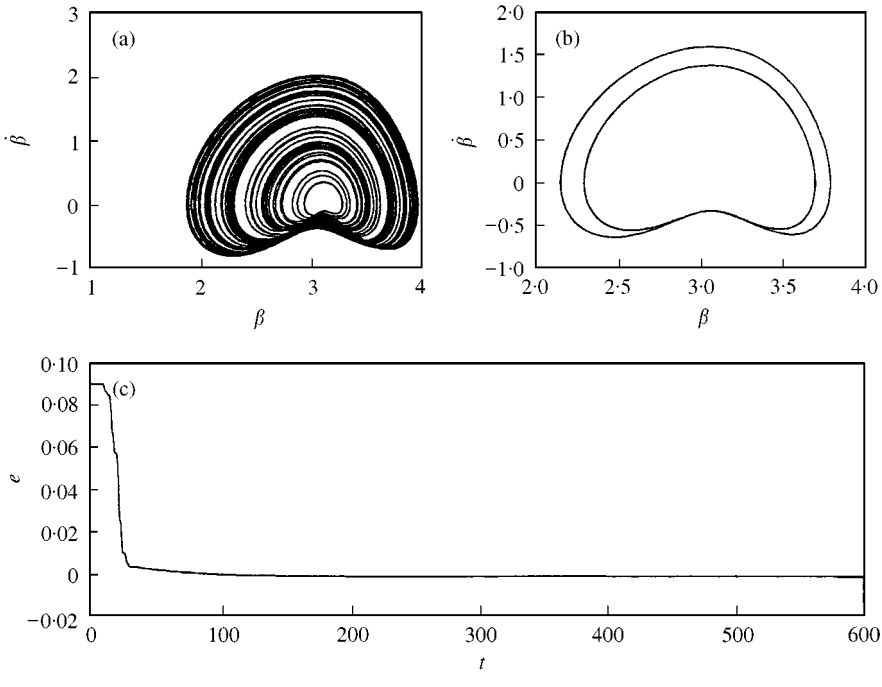

Figure 22. (a) Phase portraits before control for $\gamma = 3{\cdot}03$; (b) after control (c) error function.

Adaptive control can change chaos behavior into periodic motion. The result is shown in Figure 22 for $\gamma = 3{\cdot}03$. Figures 22(a), 22(b) and 22(b) show chaos behavior, periodic motion respectively.

13. BANG-BANG CONTROL

Define the error function as follows:

$$e(t) = X(t) - X(t - T), \tag{24}$$

where T is the external torque period. Define $V(t) = e(t)^2$ which is always positive or zero:

$$\dot{V} = 2e(t)\dot{e}(t).$$

Let $\dot{V} \leqslant 0$ then $V(t) \to 0$, $e(t) \to 0$ and $X(t) \to X(t - T)$.

By detecting equation (24) is less than or greater than zero, the control law can be determined as follows.

Assume

$$\dot{x}_1 = F_1(x_1, x_2, x_3, t) + u, \quad \dot{x}_2 = F_2(x_1, x_2, x_3, t), \quad \dot{x}_3 = F_3(x_1, x_2, x_3, t)$$

if $\|e(t)\| \leqslant \delta$, $u(t) = 0$, else if $\|e(t)\| > \delta$ then

$$u(t) = K(F_1(x_1, x_2, x_3, t) - \dot{x}_1(t - T)) \quad \text{when } e(t) > 0,$$

$$u(t) = -K(F_1(x_1, x_2, x_3, t) - \dot{x}_1(t - T)) \quad \text{when } e(t) < 0.$$

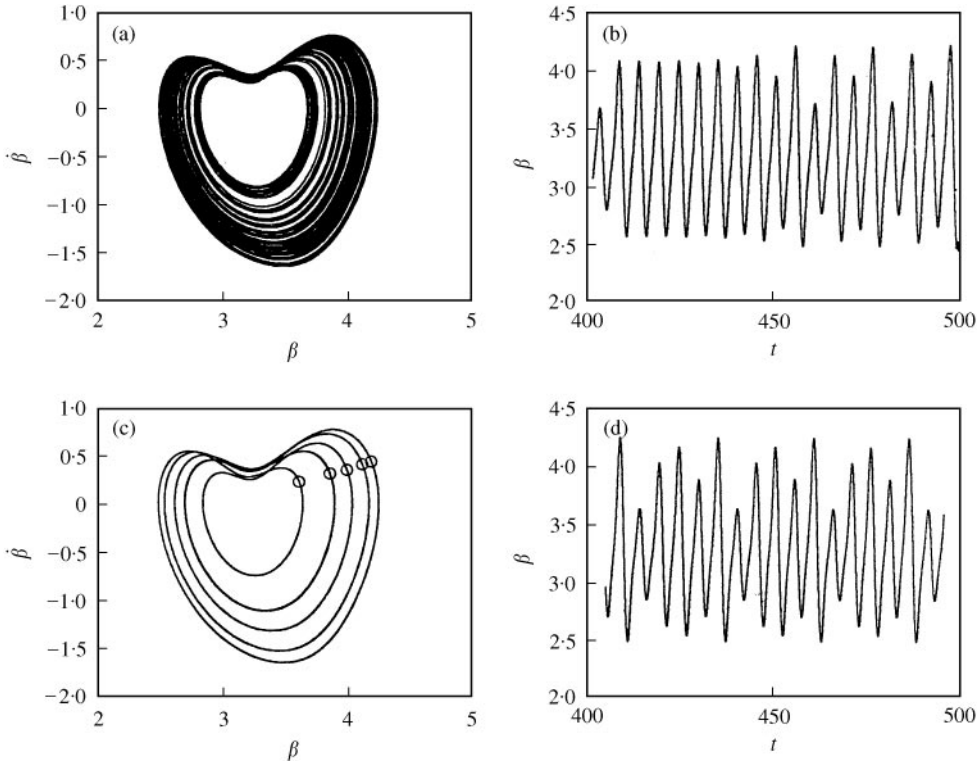

Figure 23. (a) Phase portraits; (b) time history for uncontrolled system when $\gamma = 2{\cdot}91$, (c) Phase portraits; (d) time history for controlled system when $\gamma = 2{\cdot}91$.

When the trajectory gets closer to our target periodic orbit, the control signal approaches to zero. This is why the method is called "bang–bang" control. The phase diagram of the uncontrolled system is shown in Figures 23(a), and in 23(c) the phase diagram after control is shown for $\gamma = 2{\cdot}91$. Figures 23(b) and 23(d) show time history of this system before and after control.

14. CONCLUSIONS

The dynamical system of the rigid body with vibrating support exhibits a rich variety of non-linear behavior as the parameters vary. Due to the effect of non-linearity, regular or chaotic motions may appear. In this paper, analytical, and computational methods have been employed to study the dynamical behavior of the non-linear system. The stability conditions for the rigid-body system have been found by using the Lyapunov direct method.

The incremental harmonic balance (IHB) method deals with the system which has strong non-linear terms. The phase portraits and bifurcation diagram obtained by IHB are in good agreement with the solution obtained by numerical integration method. Finally, global analysis of the basin boundary and fractal structure have been observed by the MICM method.

We have demonstrated that simple control strategies can be effectively used to suppress chaos in a non-linear dynamical system. We hope that similar control strategies can be successfully implemented for more situations.

ACKNOWLEDGMENTS

This research was supported by the National Science Council, Republic of China, under Grant No. NSC81-0401-E-009-07. We appreciate Dr S. C. Lee for his enthusiastic assistance.

REFERENCES

1. N. N. BOLOTNIK 1994 *Journal of Applied Mechanics(R)* **58**, 841–848. Inertial motion of an absolutely rigid body on two-degrees-of-freedom joint.
2. L. D. AKULENKO and D. D. LESHCHENKO 1991 *Izvestiya Akademii Nauk SSSR. MTT* **2**, 8–17. Relative oscillations and rotation of a plane articulate linkage of two rigid bodies.
3. E. A. MOKHAMED and B. A. SMOL'NIKOV 1987 *Izvestiya Akademii Nauk SSSR. MTT* **5**, 28–33. Free motion of an articulated linkage of two rigid bodies.
4. R. MUKHERJEE and D. CHEN 1993 *Journal of Guidance Control and Dynamics* **16**, 961–963. Asymptotic stability theorem for autonomous systems.
5. Z. M. GE and W. P. LIU 1999 *Japanese Journal of Applied Phy6sics* **38**, 3793–3804. Two theorems of instability with application to gimbal walk.
6. A. WOLF, J. B. SWIFT, H. L. SWINNEY and J. A. VASTANO 1985 *Physica D* **16**, 285–317. Determining Lyapunov exponent from a time series.
7. S. L. LAU and S. W. YUEN 1991 *Computer Method in Applied Mechanics and Engineer* **91**, 1109–1121. The Hopf bifurcation and limit cycle by the incremental harmonic balance method.
8. S. L. LAU and W. S. ZHANG 1992 *Journal of Applied Mechanics* **59**, 153–160. Nonlinear vibration of piecewise-linear systems by incremental harmonic balance method.
9. S. L. LAU and S. W. YUEN 1993 *Journal of Sound and Vibration* **167**, 303–316. Solution diagram of non-linear dynamic systems by IHB method.
10. Y. K. CHEUNG and S. H. CHEN 1990 *Journal of Sound and Vibration* **140**, 273–286. Application of the incremental harmonic balance method to cubic non-linearity systems.
11. Z. M. GE and S. C. LEE 1997 *Journal of Sound and Vibration* **192**, 189–206. A modified interpolated cell mapping method.
12. H. TONGUE and K. GU 1988 *Journal of Applied Mechanics* **55**, 461–466. Interpolated cell mapping of dynamical systems.
13. Y. BREIMAN and I. GOLDHIRSCH 1991 *Physical Review Letters* **66**, 2545–2548. Taming chaotic dynamics with weak periodic perturbation.
14. C. C. FUH and P. C. TUNG 1998 *Physics Letters A* **229**, 228–234. Experimental and analytical study of dither signals in a class of chaotic systems.
15. K. PYRAGAS 1992 *Physics Letters A* **170**, 421–428. Continuous control of chaos by self-controlling feedback.
16. K. PYRAGAS and A. TAMAŠEVICIUS 1993 *Physics Letters A* **180**, 99–102. Experimental control of chaos by delayed self-controlling feedback.
17. S. SINHA, R. RAMASWAMY and J. S. RAO 1990. *Physica D* **43**, 118–128. Adaptive control in nonlinear dynamics.

APPENDIX A

$$M_1 = -b(x_{20})Z(x_{20})\Omega_0^2 x_{10} + J_{11}Z(x_{20})x_{30}\Omega_0^2,$$

$$M_2 = H(x_{20})\Omega_0^2\dot{x}_{10} - \tfrac{1}{2}J(x_{20})Z(x_{20})\Omega_0^2 x_{10}^2 - R(x_{20})b(x_{20})\Omega_0^2 x_{10}^2 - J_{11}J(x_{20})\sin x_{20}$$
$$- J_{11}\gamma_0 J(x_{20})\sin\tau\sin x_{20} - J_{11}b(x_{20})\cos x_{20} - J_{11}\gamma_0 b(x_{20})\sin\tau\cos x_{20}$$
$$+ 2J_{11}R(x_{20})\Omega_0^2 x_{10}x_{30} + J_{11}b(x_{20})x_{30}^2\Omega_0^2 + k_2 J(x_{20})x_{30}\Omega_0,$$

$$M_3 = k_2 b(x_{20})\Omega_0 + J_{11}Z(x_{20})x_{10}\Omega_0^2 - 2J_{11}x_{30}J(x_{20})\Omega_0^2,$$

$$M_4 = -2A(x_{20})\dot{x}_{10}\Omega_0 + b(x_{20})Z(x_{20})\Omega_0 x_{10}^2 - k_2 b(x_{20})x_{320} - 2J_{11}Z(x_{20})x_{10}x_{30}\Omega_0 + 2J_{11}J(x_{20})x_{30}^2\Omega_0 - J_{11}k_1 x_{10},$$

$$M_5 = J_{11}b(x_{20})\sin\tau\sin x_{20},$$

$$M_6 = \tfrac{1}{2}b(x_{20})Z(x_{20})\Omega_0^2 x_{10}^2 + J_{11}\, b(x_{20})\sin x_{20} + J_{11}\gamma_0 b(x_{20})\sin\tau\sin x_{20} - k_2 b(x_{20})x_{30}\Omega_0 - J_{11}Z(x_{20})x_{10}x_{30}\Omega_0^2 + J_{11}J(x_{20})\Omega_0^2 x_{30}^2 - J_{11}k_1\Omega_0 x_{10} - \Omega_0^2 A(x_{20})\dot{x}_{10},$$

$$M_7 = b(x_{20})Z(x_{20})\Omega_0^2 x_{30} + k_1 b(x_{20})\Omega_0 - K(x_{20})Z(x_{20})x_{10}\Omega_0^2,$$

$$M_8 = H(x_{20})\Omega_0^2\dot{x}_{30} - J^2(x_{20})x_{30}^2\Omega_0^2 + b(x_{20})x_{30}^2\Omega_0^2 + J(x_{20})Z(x_{20})x_{30}\Omega_0^2 x_{10} + 2R(x_{20})b(x_{20})x_{30}\Omega_0^2 x_{10} + k_1 J(x_{20})\Omega_0 x_{10} - \tfrac{1}{2}Z^2(x_{20})\Omega_0^2 x_{10}^2 - R(x_{20})K(x_{20})\Omega_0^2 x_{10}^2 - J_{11}Z(x_{20})\sin x_{20} - J_{11}Z(x_{20})\gamma_0\sin\tau\sin x_{20} - J_{11}K\gamma_0\sin\tau\cos x_{20} + k_2 Z(x_{20})\Omega_0 x_{30} - J_{11}K(x_{20})\cos x_{20},$$

$$M_9 = -2b(x_{20})J(x_{20})x_{30}\Omega_0^2 + bZ(x_{20})\Omega_0^2 x_{10} + k_2 K(x_{20})\Omega_0,$$

$$M_{10} = -2A(x_{20})\Omega_0\dot{x}_{30} + 2b(x_{20})J(x_{20})\Omega_0 x_{30}^2 - 2b(x_{20})Z(x_{20})\Omega_0 x_{10}x_{30} - k_1 b(x_{20})x_{10} + K(x_{20})Z(x_{20})x_{10}^2\Omega_0 - k_2 K(x_{20})x_{30},$$

$$M_{11} = J_{11}K(x_{20})\sin\tau\sin x_{20},$$

$$M_{12} = b(x_{20})J(x_{20})\Omega_0^2 x_{30}^2 - b(x_{20})Z(x_{20})x_{10}x_{30}\Omega_0^2 - k_1 b(x_{20})\Omega_0 x_{10} + \tfrac{1}{2}K(x_{20})Z(x_{20})\Omega_0^2 x_{10}^2 + J_{11}K(x_{20})\gamma\sin\tau\sin x_{20} - k_2 K(x_{20})\Omega_0 x_{30} - A(x_{20})\Omega_0^2\dot{x}_{30} + J_{11}K(x_{20})\sin x_{20}$$

where

$$K(x_{20}) = J_{22}\sin^2 x_{20} + J_{33}\cos^2 x_{20} - J_{23}\sin 2x_{20},$$

$$b(x_{20}) = J_{12}\sin x_{20} + J_{13}\cos x_{20},$$

$$Z(x_{20}) = (J_{22} - J_{33})\sin 2x_{20} - 2J_{23}\cos 2x_{20},$$

$$J(x_{20}) = J_{12}\cos x_{20} - J_{13}\sin x_{20},$$

$$A(x_{20}) = K(x_{20})J_{11} - b^2(x_{20}),$$

$$H(x_{20}) = Z(x_{20})J_{11} - 2b(x_{20})J(x_{20}),$$

$$R(x_{20}) = (J_{22} - J_{33})\cos 2x_{20} + 2J_{23}\sin 2x_{20},$$

$$\mathbf{G} = \begin{bmatrix} A(x_{20})\Omega_0^2 & 0 & 0 \\ 0 & 1 & 0 \\ 0 & 0 & A(x_{20})\Omega_0^2 \end{bmatrix}, \quad \mathbf{K} = \begin{bmatrix} M_1 + J_{11}k_1\Omega_0 & M_2 & M_3 \\ 0 & 0 & -1 \\ M_7 & M_8 & M_9 \end{bmatrix},$$

$$\mathbf{R} = \begin{bmatrix} M_6 \\ x_{30} - \dot{x}_{20} \\ M^{12} \end{bmatrix}, \quad \mathbf{F} = \begin{bmatrix} M_4 \\ 0 \\ M_{10} \end{bmatrix}, \quad \mathbf{D}_1 = \begin{bmatrix} M_5 \\ 0 \\ M_{11} \end{bmatrix},$$

$$\mathbf{D} = [1, \cos\tfrac{1}{q}\tau_I, \cos\tfrac{2}{q}\tau_I, \dots, \cos\tfrac{N}{q}\tau_I, \sin\tfrac{1}{q}\tau_I, \sin\tfrac{2}{q}\tau_I, \dots, \sin\tfrac{N}{q}\tau_I],$$

$$\mathbf{A} = [a_0, a_1, a_2, \dots, a_N, b_1, b_2, \dots, b_N]^{\mathrm{T}},$$

$$\Delta\mathbf{A} = [\Delta\dot{a}_0, \Delta a_1, \Delta a_2, \dots, \Delta a_N, \Delta b_1, \Delta b_2, \dots, \Delta b_N]^{\mathrm{T}},$$

$$\mathbf{B} = [c_0, c_1, c_2, \dots, c_N, d_1, d_2, \dots, d_N]^{\mathrm{T}},$$

$$\Delta\mathbf{B} = [\Delta c_0, \Delta c_1, \Delta c_2, \dots, \Delta c_N, \Delta d_1, \Delta d_2, \dots, \Delta d_N]^{\mathrm{T}},$$

$$\mathbf{C} = [e_0, e_1, e_2, \dots, e_N, f_1, f_2, \dots, f_N]^{\mathrm{T}},$$

$$\Delta\mathbf{C} = [\Delta e_0, \Delta e_1, \Delta e_2, \dots, \Delta e_N, \Delta f_1, \Delta f_2, \dots, \Delta f_N]^{\mathrm{T}},$$

$$\mathbf{M} = \int_0^{2\pi} \mathbf{P}^{\mathrm{T}}[\mathbf{G}\dot{\mathbf{P}} + \mathbf{K}\mathbf{P}]\,\mathrm{d}\tau,$$

$$\bar{\mathbf{R}} = \int_0^{2\pi} \mathbf{P}^{\mathrm{T}}\mathbf{R}\,\mathrm{d}\tau.$$